The effects of nonuniform magnetic field strength on density flux and test particle transport in drift wave turbulence

J. M. Dewhurst,[1,a)] B. Hnat,[1] and R. O. Dendy[1,2]
[1]*Centre for Fusion, Space and Astrophysics, Department of Physics, Warwick University, Coventry CV4 7AL, United Kingdom*
[2]*Euratom/UKAEA Fusion Association, Culham Science Centre, Abingdon, Oxfordshire OX14 3DB, United Kingdom*

(Received 2 April 2009; accepted 22 June 2009; published online 14 July 2009)

The extended Hasegawa–Wakatani equations generate fully nonlinear self-consistent solutions for coupled density n and vorticity $\nabla^2\phi$, where ϕ is electrostatic potential, in a plasma with background density inhomogeneity $\kappa=-\partial \ln n_0/\partial x$ and magnetic field strength inhomogeneity $C=-\partial \ln B/\partial x$. Finite C introduces interchange effects and ∇B drifts into the framework of drift turbulence through compressibility of the $E\times B$ and diamagnetic drifts. This paper addresses the direct computation of the radial $E\times B$ density flux $\Gamma_n=-n\partial\phi/\partial y$, tracer particle transport, the statistical properties of the turbulent fluctuations that drive Γ_n and tracer motion, and analytical underpinnings. Systematic trends emerge in the dependence on C of the skewness of the distribution of pointwise Γ_n and in the relative phase of density-velocity and density-potential pairings. It is shown how these effects, together with conservation of potential vorticity $\Pi=\nabla^2\phi-n+(\kappa-C)x$, account for much of the transport phenomenology. Simple analytical arguments yield a Fickian relation $\Gamma_n=(\kappa-C)D_x$ between the radial density flux Γ_n and the radial tracer diffusivity D_x, which is shown to explain key trends in the simulations. © *2009 American Institute of Physics*. [DOI: 10.1063/1.3177382]

I. INTRODUCTION

Understanding the transport of particles and energy in turbulent plasma is fundamentally important to the goal of magnetically confined nuclear fusion. This is particularly true in the edge region of a tokamak, where turbulent transport responds to, and also determines, the radial density and temperature profiles. Edge turbulence, together with magnetohydrodynamic instabilities, also determines the flux of particles and energy across the last closed magnetic flux surface, and hence to the divertor or the first wall. Experimental measurements in the edge plasma region suggest universal statistical properties in the fluctuations of plasma parameters (see, for example, Refs. 1–7). Some aspects of the proposed universality may apply to all three of the leading toroidal magnetic confinement systems: conventional aspect ratio tokamaks, spherical tokamaks, and stellarators.

It is generally agreed that the drift wave and interchange instabilities are key mechanisms for the generation of edge turbulence. Models including such instabilities, derived from first principles, can explain many observed physical properties. Drift wave turbulence is dominated by low frequency waves which are driven unstable by gradients in density or temperature, see Ref. 8 for a review. The parallel electron current with an adiabatic or nonadiabatic electron response provides an effective energy transfer channel from the edge pedestal and into the flow. Drift wave phenomenology is purely electrostatic, and generally the magnetic field is assumed to be uniform. In tokamaks, however, the toroidal magnetic field strength is nonuniform and declines with radial distance from the axis of symmetry. The inclusion of this magnetic field gradient leads to a nonvanishing divergence of diamagnetic velocity, associated with compressible effects, and the appearance of the interchange instability. In toroidal geometry, interchange modes have destabilizing effects in the region where the vectors ∇B and the radius of curvature are parallel to the pressure gradient (low field side) and have stabilizing effects on the high field side. This alters the properties of the turbulence, allowing the excitation of interchange-type ballooning modes. Plasma particles, following helical magnetic field lines, experience both interchange-stable and interchange-unstable regions and their behavior is averaged over these different regimes of turbulence.

In this paper we investigate the effects of nonuniform background magnetic field strength on the turbulence and the transport of passive test particles using direct numerical simulation of a two-dimensional (2D) turbulent system. Our model of drift wave turbulence is an extended form of the Hasegawa–Wakatani (HW) equations[9] that includes magnetic field inhomogeneity in the radial direction and the resulting interchange driven modes.[10] We refer to this as the extended Hasegawa–Wakatani (EHW) model. This model was studied in three-dimensional (3D) by Sugama *et al.*[11] and in 2D in Refs. 12 and 13, for example; see also Ref. 8. The HW model is a paradigmatic description of electrostatic potential ϕ and electron density n in the edge region of a tokamak plasma that has a nonuniform background density and uniform equilibrium magnetic field. It generalizes the simpler Hasegawa–Mima (HM) equation[14] to include a nonadiabatic electron response due to parallel resistivity. This gives rise to an instability which is absent in the HM equation; in this respect the HW model provides a more complete description of drift wave turbulence. We focus on

a)Electronic mail: j.m.dewhurst@warwick.ac.uk.

the physically relevant turbulent radial density flux Γ_n and examine how its distribution changes with the parameter controlling the magnetic field inhomogeneity $C=-\partial \ln B/\partial x$. Changes in the distribution are determined by the relative phase difference between density n and radial velocity v_x (or potential ϕ).

A complementary perspective on the turbulence can be obtained through the study of passive tracer particles.[15–27] Using the HM equation as the turbulence model, the transport of passive test particles was studied in Refs. 15–19. Test particle transport in the HW model was studied in Refs. 20–24 and a recent overview can be found in Ref. 25. Here we report on the influence of the magnetic field inhomogeneity that is included in the EHW model. The rate of radial transport of test particles is found to increase monotonically with C, while the rate of poloidal transport decreases monotonically. For large negative values of C, correlations in the flow persist for long times, and the radial transport becomes subdiffusive while the poloidal transport becomes superdiffusive. The rate of radial diffusive test particle transport and the average $E\times B$ density flux are linked by a simple expression which we derive in the form of Fick's law.

II. MODEL EQUATIONS

The EHW equations for density n and vorticity $\nabla^2\phi$, where ϕ is the electrostatic potential, are[8,10]

$$\frac{\partial n}{\partial t}=-\kappa\frac{\partial \phi}{\partial y}+\alpha(\phi-n)+[n,\phi]+C\frac{\partial}{\partial y}(\phi-n)+D\nabla^2 n, \tag{1}$$

$$\frac{\partial}{\partial t}(\nabla^2\phi)=\alpha(\phi-n)+[\nabla^2\phi,\phi]-C\frac{\partial n}{\partial y}+\mu\nabla^2(\nabla^2\phi), \tag{2}$$

where we use the Poisson bracket notation for nonlinear terms $[A,B]=(\partial A/\partial x)(\partial B/\partial y)-(\partial A/\partial y)(\partial B/\partial x)$. The equations have been normalized using

$$\frac{e\tilde{\phi}}{T_e}\to\phi,\quad \frac{\tilde{n}}{n_0}\to n,\quad \omega_{ci}t\to t,\quad \frac{x,y}{\rho_s}\to x,y, \tag{3}$$

where fluctuating quantities are expressed with tildes, T_e is electron temperature, ω_{ci} is ion gyrofrequency, and $\rho_s=\sqrt{m_iT_e}/eB$ is hybrid Larmor radius. Dissipation terms of the form $\nabla^2 f$ are added to the equations for numerical reasons, and D and μ are dissipation coefficients. The x and y directions are identified, respectively, with the radial and poloidal directions in a tokamak, and the magnetic field is assumed to point in the z direction with its inhomogeneity in the x direction, $\mathbf{B}=B(x)\hat{\mathbf{z}}$. We assume that $\kappa=-\partial \ln n_0/\partial x$, controlling the background density profile $n_0(x)$, and $C=-\partial \ln B/\partial x$, controlling the gradient of $B(x)$, are constants. The model is cast into 2D by assuming a single parallel wave number k; then the parameter α controls the strength of the resistive coupling between n and ϕ through the parallel current,

$$\alpha=\frac{T_ek^2}{n_0e^2\eta\omega_{ci}}, \tag{4}$$

where η is electron resistivity. The standard HW equations are recovered from the EHW equations when $C=0$. The extra terms at finite C represent interchange forcing due to the nonuniform magnetic field and enter the equations through compressibility of the $E\times B$ and diamagnetic velocities. In the limit $\alpha\gg 1$ the coupling is adiabatic ($n=\phi$ in our normalized units) and the HW equations reduce to the HM equation.

With $D=\mu$, the EHW equations can be rewritten in the form of a diffusion equation, $d\Pi/dt=D\nabla^2\Pi$, where Π is the potential vorticity,

$$\Pi=[\nabla^2\phi-n+(\kappa-C)x], \tag{5}$$

and $d/dt=\partial/\partial t+[\phi,]$ is the convective derivative associated with $E\times B$ drift along the contours of ϕ. In the inviscid limit ($D=\mu=0$) the potential vorticity is a Lagrangian conserved quantity,[8] $d\Pi/dt=0$. The approximate conservation of this quantity plays an important role in the dynamics of turbulent structures, as discussed later.

Evolution equations for the energy E,

$$E=\frac{1}{2}\int[n^2+(\nabla\phi)^2]dV, \tag{6}$$

and generalized enstrophy W,

$$W=\frac{1}{2}\int(n-\nabla^2\phi)^2dV, \tag{7}$$

can be written

$$\frac{d}{dt}E=\kappa\Gamma_{n0}-D_\alpha,\quad \frac{d}{dt}W=(\kappa-C)\Gamma_{n0}, \tag{8}$$

where we have neglected numerical dissipation. Here,

$$\Gamma_{n0}=-\int n\frac{\partial\phi}{\partial y}dV \tag{9}$$

is the total radial $E\times B$ density flux, which acts as the system's source, while

$$D_\alpha=\alpha\int(\phi-n)^2dV \tag{10}$$

is a sink term due to the parallel current. By Eq. (8), $\kappa>C$ is required for Γ_{n0} to be a source of generalized enstrophy W. Note that in the HM limit ($\alpha\gg 1$) energy is conserved since $n=\phi$, consistent with $\Gamma_{n0}=D_\alpha=0$.

Linearizing and Fourier decomposing Eqs. (1) and (2), we obtain for plane waves of $\sim\exp[i(k_xx+k_yy-\omega t)]$,

$$\omega n_k=(\kappa-C)k_y\phi_k+Ck_yn_k+i\alpha(\phi_k-n_k), \tag{11}$$

$$\omega k^2\phi_k=-Ck_yn_k-i\alpha(\phi_k-n_k). \tag{12}$$

Eliminating n_k/ϕ_k we obtain the dispersion relation,

$$\omega^2 k^2 + \omega[i\alpha(1+k^2) - Ck_y k^2] + k_y(\kappa - C)[Ck_y - i\alpha] = 0, \tag{13}$$

which, in the limit $\alpha \gg 1$, becomes

$$\omega = \frac{(\kappa - C)k_y}{1+k^2}, \tag{14}$$

which is the usual drift-wave dispersion relation modified by a factor of $(\kappa - C)/\kappa$. In the long wavelength limit $(k^2 \to 0)$, the linear drift waves propagate in the poloidal y direction with phase velocity,

$$U = \kappa - C. \tag{15}$$

Restoring the units, $U = u_{de} - u_{\nabla B}$, where $u_{de} = -(T_e/eBn_0) \times (\partial n_0/\partial x)$ is the electron diamagnetic drift velocity and $u_{\nabla B} = -(T_e/eB^2)(\partial B/\partial x)$ is the modification due to ∇B effects. Since the ratio of two complex numbers can be expressed as an amplitude and a phase shift, an expression for the linear phase shifts between n and ϕ can be found by eliminating ω in Eqs. (11) and (12) instead of n_k/ϕ_k. In the long wavelength limit, we obtain

$$\theta = \arctan\left(\frac{Ck_y}{\alpha}\right). \tag{16}$$

Thus, in the linear regime, the parameter C alters the poloidal velocity of the drift waves and the phase shift between density n and potential ϕ. In the nonlinear regime, as we shall see, these features are retained.

III. NUMERICAL METHODS

We solve Eqs. (1) and (2) on a square of length $L=40$ using 256×256 grid nodes with periodic boundary conditions. We use the third order Karniadakis time integration scheme[28] and the finite differences method for spatial discretization, with the Poisson bracket being computed through Arakawa's[29] method. This combination of numerical methods was introduced in Ref. 30, tested in Ref. 31, and discussed in detail in Ref. 32. Runs of the code are started with low-amplitude random noise. Linear drift waves are excited and grow exponentially until nonlinear effects become important. Eventually, a quasistationary turbulent state dominated by turbulent vortex structures is reached. This is examined in Sec. IV.

For the test particle studies described in Sec V, 10 000 particles are initialized at random positions throughout the domain once the quasistationary turbulent state has been reached. The test particle equation of motion is $\partial \mathbf{r}/\partial t = \mathbf{v}_E(\mathbf{r})$, where $\mathbf{v}_E(\mathbf{r})$ is the local $E \times B$ velocity and the third order Karniadakis scheme[28] is used for time integration. In normalized units, the $E \times B$ velocity is

$$\mathbf{v}_E = \left(-\frac{\partial \phi}{\partial y}, \frac{\partial \phi}{\partial x}\right). \tag{17}$$

We use bilinear interpolation to calculate the potential ϕ at points away from grid nodes. We calculate a running diffusion coefficient in the radial x and poloidal y directions separately,

$$D_x(t) = \frac{X(t)^2}{2t}, \quad D_y(t) = \frac{Y(t)^2}{2t}. \tag{18}$$

Here $X(t)^2 = \langle [x(t) - \langle x(t) \rangle]^2 \rangle$, $Y(t)^2 = \langle [y(t) - \langle y(t) \rangle]^2 \rangle$, and $[x(t), y(t)]$ is the position of the particle with respect to its initial position; angular brackets denote an ensemble average over the 10 000 test particles. For an ordinary diffusive process the running diffusion coefficient will reach a value independent of time since $X(t)^2 \sim t$. More generally the transport may be "anomalous" and $X(t)^2 \sim t^\sigma$, where $0 < \sigma < 1$ implies subdiffusion, $1 < \sigma < 2$ implies superdiffusion, and $\sigma = 2$ is ballistic.

We note from Eq. (17) that contours of equipotential ϕ are stream lines of $\mathbf{v}_E$. Therefore, on time scales shorter than their lifetime, the turbulent structures are impervious to test particles. Conversely, test particles can be trapped by the structures and the dynamics of the structures will affect the dispersion of the test particles. In Ref. 21 it was shown that passive test particle transport in the HW model is essentially a normal diffusive process due to trapping and detrapping of the test particles by the turbulent structures. It was also shown that poloidal diffusion is stronger than radial, $D_y > D_x$. In Ref. 22 increasing the coupling parameter α was shown to decrease the rate of radial test particle transport. The effect of finite ion inertia and the polarization drift was studied in Ref. 23, and the intermittent nature of test particle transport in the HW model was studied in Ref. 24. Here, we focus on the effects of the magnetic field inhomogeneity incorporated in the EHW model.

IV. PROPERTIES OF THE TURBULENCE

We are interested in the effect of changing the magnetic field inhomogeneity [i.e., changing the value of the parameter C in Eqs. (1) and (2)] on the transport of test particles. We therefore set $\alpha = 0.5$, $\kappa = 1$, $\mu = D = 0.01$ throughout. We choose the set $C = [-0.3, 0, 0.3]$ as representative of different locations with respect to an equilibrium magnetic field. When the parameters κ and C are opposite in sign, the gradients of magnetic field strength and of background density point in opposite directions, as is the case on the inboard side of a tokamak. When κ and C share the same sign, the gradients of magnetic field strength and of background density point in the same direction, as is the case on the outboard side of a tokamak. In the latter case, perturbations in density lead to radial $E \times B$ motion due to the ∇B plasma polarization (see Ref. 4 for example) and the plasma is said to be interchange unstable. In the former case, the plasma is interchange stable. In reality, the inboard and outboard sides of a tokamak are connected by helically wound magnetic field lines. This 3D effect results in ballooning type modes and is beyond the scope of this paper.

Figure 1 shows the typical snapshots of the potential ϕ in the quasistationary saturated turbulent state for $C = [-0.3, 0, 0.3]$. In each case, the turbulence is dominated by vortex structures. Contours represent $E \times B$ velocity stream lines which test particles follow exactly.

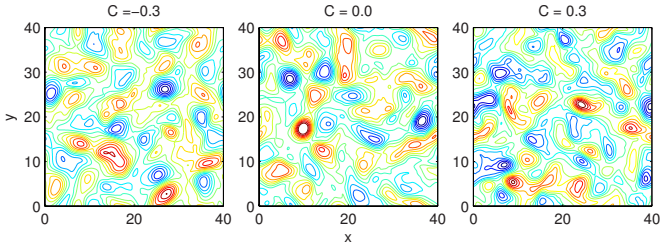

FIG. 1. (Color online) Contours of potential ϕ in the quasistationary saturated turbulent state of the EHW system for different values of $C=-\partial \ln B/\partial x$.

A. Probe measurements

In experiment, properties of the turbulence are often determined by probe measurements of the turbulent $E\times B$ radial density flux,

$$\Gamma_n = nv_x = -n\frac{\partial \phi}{\partial y}. \tag{19}$$

We therefore record this quantity along with density n, potential ϕ, and radial velocity $v_x=-\partial\phi/\partial y$ at one grid node (i.e., pointwise) for the entire duration of the quasistationary turbulent state of the EHW system. From the Γ_n time series we compute its probability density function (PDF) $P(\Gamma_n)$ and quantify the departures of the distribution from Gaussian with skewness $S=\langle\Gamma_n^3\rangle/\langle\Gamma_n^2\rangle^{3/2}$, measuring asymmetry, and kurtosis $K=\langle\Gamma_n^4\rangle/\langle\Gamma_n^2\rangle^2$, measuring peakedness; a Gaussian PDF has $S=0$ and $K=3$.

Figure 2(a) shows the PDFs $P(\Gamma_n)$ for the three different values of $C=-\partial \ln B/\partial x$. All three PDFs are clearly non-Gaussian and are skewed toward positive radial flux. We note that non-Gaussian PDFs of the turbulent flux and/or density are regularly measured in the edge region of experiments, see Refs. 1–7 and 33 for example. In Fig. 2(b), we plot the skewness of the PDFs for a wider range of C. Increasing the parameter C, which corresponds to steepening the decline in magnetic field strength with radial distance, monotonically increases the positive radial skewness of Γ_n.

In Fig. 2(c) we plot the skewness and kurtosis of the distributions of pointwise measurements of density n, potential ϕ, and radial velocity v_x for different values of C in the EHW system. These quantities are very close to Gaussian for the full range of C with radial velocity v_x showing the largest departure from Gaussian in its kurtosis. For the case where the amplitudes of the fluctuations in radial velocity v_x and density n are exactly Gaussian, the PDF of radial turbulent flux $\Gamma_n=nv_x$ can be shown to be[33]

$$P(\Gamma_n) = \frac{1}{\pi}\frac{\sqrt{1-\gamma^2}}{\sigma_v\sigma_n}K_0\left(\frac{|\Gamma_n|}{\sigma_v\sigma_n}\right)\exp\left(-\gamma\frac{\Gamma_n}{\sigma_v\sigma_n}\right), \tag{20}$$

where σ_v and σ_n are the standard deviations of velocity and density fluctuations, K_0 is the modified Bessel function of the second kind, and γ is a parameter that measures the correlation between v_x and n,

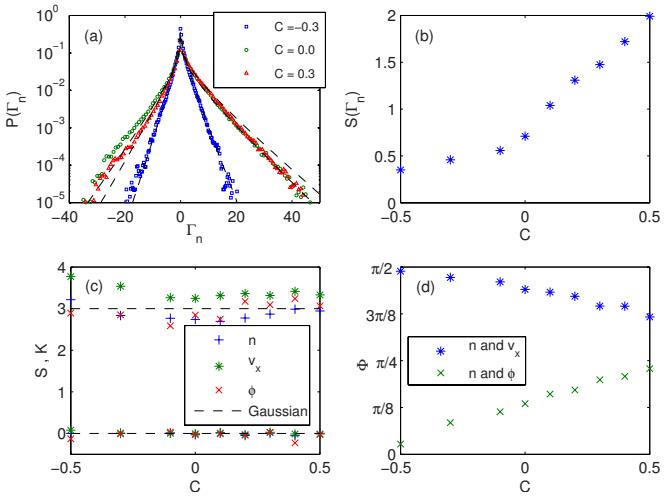

FIG. 2. (Color online) (a) PDFs and (b) skewness of PDFs of the pointwise radial density flux $\Gamma_n=nv_x$ for different values of C. The dashed lines over the PDFs are the PDFs calculated using Eqs. (20) and (21) and probe data from the simulation. (c) Skewness and kurtosis of PDFs of pointwise density n, radial velocity v_x, and potential ϕ. (d) Relative phase between n and v_x and between n and ϕ for different values of C.

$$\gamma = -\frac{\langle v_x n\rangle}{\langle v_x^2\rangle^{1/2}\langle n^2\rangle^{1/2}} \equiv -\cos\Phi, \tag{21}$$

where Φ is the average relative phase between v_x and n. The averaged flux is[33]

$$\Gamma_{n0} = -\frac{\gamma}{1-\gamma^2}\langle v_x^2\rangle^{1/2}\langle n^2\rangle^{1/2}, \tag{22}$$

and the skewness of the PDF can be calculated[33] as

$$S = -2\gamma\frac{3+\gamma^2}{(1+\gamma^2)^{3/2}}, \tag{23}$$

which depends on the parameter γ only. In Fig. 2(d) we plot the relative phase Φ between v_x and n, and also between ϕ and n, showing that Φ changes roughly linearly with C. We conclude that changing C alters the relative phase between fluctuations in density n and potential ϕ, which leads to the observed change in the skewness of the flux PDF. We note from Eq. (9) that an increase in the phase difference between n and ϕ should lead to an increase in the rate of radial $E\times B$ transport. A plot of the average flux Γ_{n0} as a function of C is displayed below in Fig. 7(b). In Fig. 2(a) we overlay with dashed lines the PDFs calculated using Eqs. (20) and (21) and probe data from the simulation. Moderately good agreement is found with the biggest departures occurring for large positive values of Γ_n when $C=0.3$ and large negative values of Γ_n when $C=0$. This indicates that the quantities v_x and n are indeed close to Gaussian; however, large fluctuations may follow a different distribution.

B. Propagation of nonlinear structures

Since test particles follow the contours of the potential, the dynamics of the turbulent structures govern the dispersion of test particles. Figure 3 illustrates the effect of the parameter C on the dynamics of turbulent structures. We start

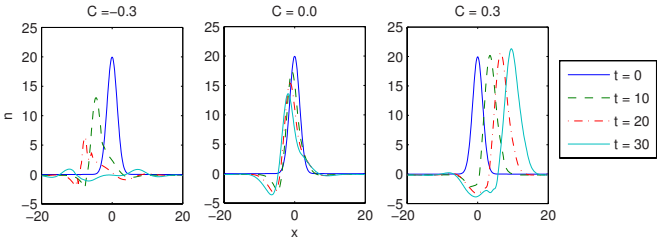

FIG. 3. (Color online) Radial evolution of density n of nonlinear structures for different values of $C=-\partial \ln B/\partial x$. The directions of the gradients of background magnetic field and density are opposed for negative C and coincident for positive C.

the simulation with a Gaussian pulse monopole structure, shown as a dark gray (blue online) solid line in Fig. 3, with $n=\phi$ in the center of the computational box, whose positive amplitude is large enough to cause nonlinear effects. We follow this structure and show in Fig. 3 the radial evolution of its density n for $C=[-0.3,0.0,0.3]$. For the standard HW case $(C=0)$ the structure propagates slowly in the negative x direction and exponentially decays slowly with time, in agreement with Ref. 34. For EHW with $C=-0.3$ the structure propagates in the negative x direction but decays at a much faster rate. For $C=0.3$ the structure propagates in the positive x direction—down the background density gradient—and grows in time. When $C=0.3$, negative amplitude nonlinear structures propagate in the negative x direction and grow in time; when $C=-0.3$ they propagate in the positive x direction and decay with time. Thus when $C=0.3$, nonlinear perturbations of density and radial velocity are correlated, and when $C=-0.3$ they are anticorrelated. Insofar as the fully developed turbulence approximates to Gaussian statistics, it follows from Eqs. (21) and (23) that the positive correlation of density and radial velocity will lead to a positive event in the time series of radial flux Γ_n and an increase in the skewness of the PDF $P(\Gamma_n)$. Similarly, negative correlation leads to negative flux events and lower skewness.

Figure 4 shows how the radial u_x and poloidal u_y velocities of the positive amplitude structure, shown in Fig. 3, change for a wider range of C. We find that the radial velocity increases with C while the poloidal velocity decreases with C. We note that in the radial x direction, positive and negative amplitude structures propagate in opposite directions, so that the radial velocity of a negative amplitude structure is approximately $-u_x$. In the poloidal y direction, however, positive and negative amplitude structures propagate in the same direction with the same velocity u_y. Thus the change in u_y with C may be understood in terms of the linear approximation embodied in Eq. (15): increasing C decreases the poloidal flow velocity. In the fully developed turbulence we also find that increasing C decreases the poloidal flow velocity. Further understanding of the radial propagation of structures can be obtained by considering the potential vorticity Π defined in Eq. (5).[22,34] Taking the time derivative of Eq. (5) gives

$$\frac{d}{dt}x \equiv u_x = -\frac{\partial \phi}{\partial y} = -\frac{1}{\kappa - C}\frac{d}{dt}\zeta, \tag{24}$$

where $\zeta=\nabla^2\phi-n$ is the fluid part of the potential vorticity and u_x is the radial component of the $E\times B$ velocity of the structure. We note that $(\kappa-C)$ must be positive by Eq. (8), and negative vorticity $\nabla^2\phi$ is associated with positive density

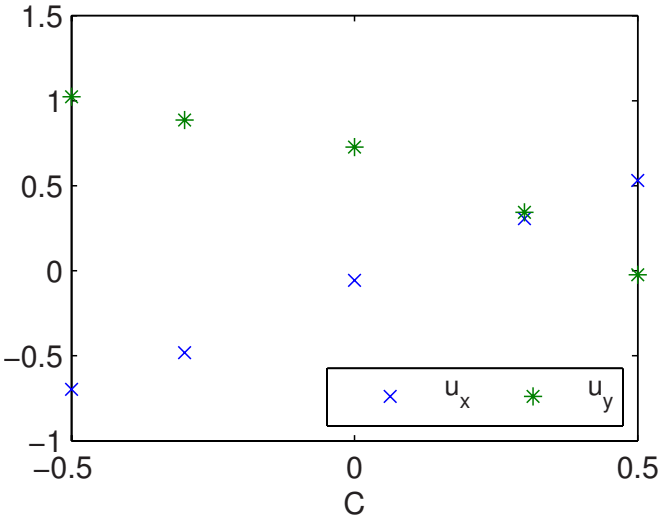

FIG. 4. (Color online) Radial u_x and poloidal u_y velocity components of positive amplitude nonlinear structures shown in Fig. 3 for different values of C.

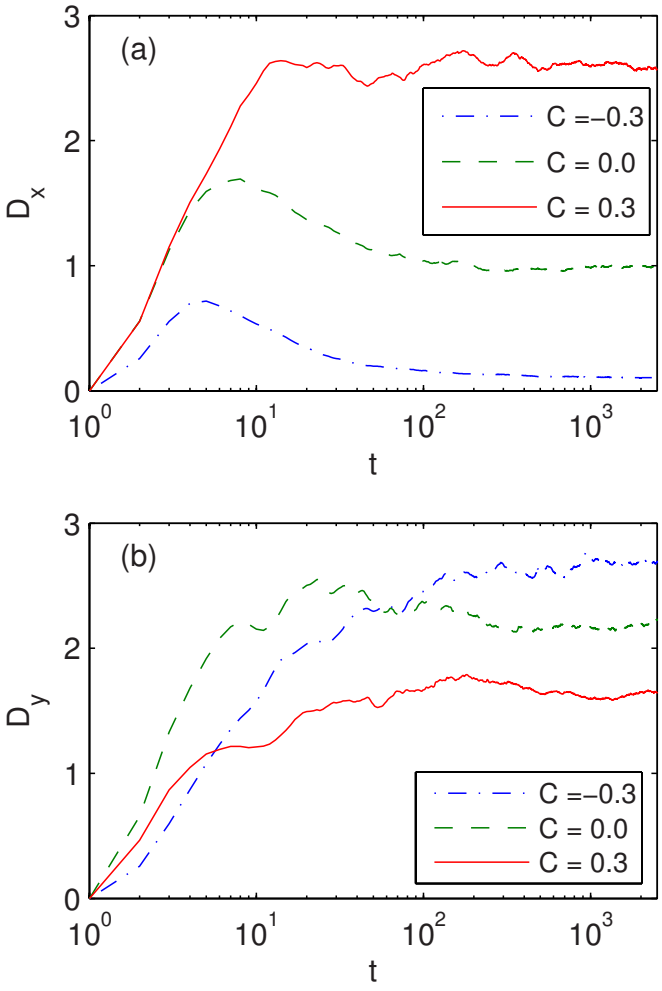

FIG. 5. (Color online) Plots of running diffusion coefficient (a) D_x and (b) D_y vs time for different values of C.

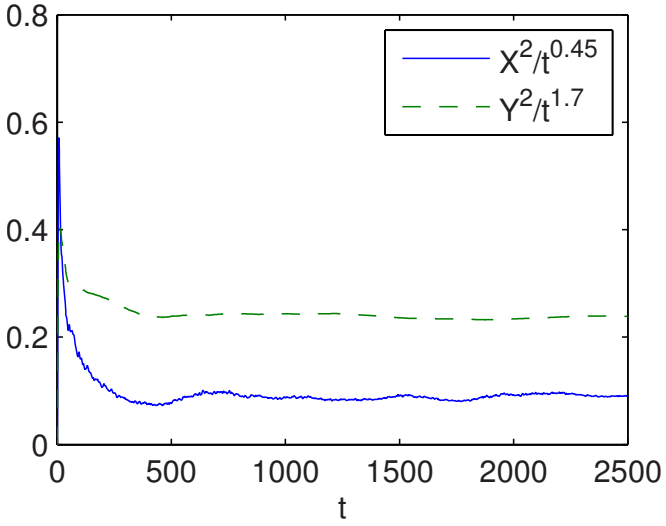

FIG. 6. (Color online) Plots of $X^2/t^{0.45}$ and $Y^2/t^{1.7}$ vs time for $C=-0.5$ showing subdiffusion in x and superdiffusion in y.

structures and vice versa.[34] In the inviscid limit, a fluid structure will propagate consistent with Eq. (24) in order to keep Π constant. Due to the trapping effects of the turbulent structures, we expect that changes in the dynamics of the turbulent structures will affect the rate of diffusion of test particles. Also, a homogeneous poloidal flow can enhance the poloidal transport and decrease the radial transport.[35]

V. TEST PARTICLE TRANSPORT

Having established that the parameter C, controlling the radial magnetic field gradient, alters the turbulence in significant ways, we now turn to the transport of test particles. In Fig. 5 we plot D_x and D_y as functions of time for $C=[-0.3,0.0,0.3]$. In all cases, after a short initial ballistic phase, the running diffusion coefficient asymptotically tends to a value independent of time, indicating a diffusive process. Increasing the parameter C tends to increase the radial diffusion coefficient D_x and decrease the poloidal one D_y. For $C=0$ and $C=-0.3$ we find that the poloidal diffusion is stronger than the radial, in agreement with Ref. 21; however, for $C=0.3$ this anisotropy is reversed and the radial diffusion dominates. In Fig. 6 we plot $X^2/t^{0.45}$ and $Y^2/t^{1.7}$ versus time for $C=-0.5$. We find that after an initial phase, these quantities become time independent, indicating that the radial test particle transport is subdiffusive with exponent $\sigma\approx 0.45$ and the poloidal transport is superdiffusive with $\sigma\approx 1.7$. Interestingly, poloidal superdiffusion with $\sigma=1.7$ was found for test particle transport in quasistationary HM turbulence; see Fig. 2(b) of Ref. 17.

Figure 7(a) displays the time-independent values of D_x and D_y for a wider range of C (for cases where the transport is diffusive). We find that D_x increases and D_y decreases with C. We also plot the total radial density flux Γ_{n0} [defined in Eq. (9)] averaged over the computational box in Fig. 7(b). Extending the arguments in Ref. 22, Γ_{n0} and D_x can be linked through conservation of potential vorticity Π. It follows from Eq. (24) that $\langle(dx/d\zeta)^2\rangle=(\kappa-C)^{-2}$, from Eq. (18)

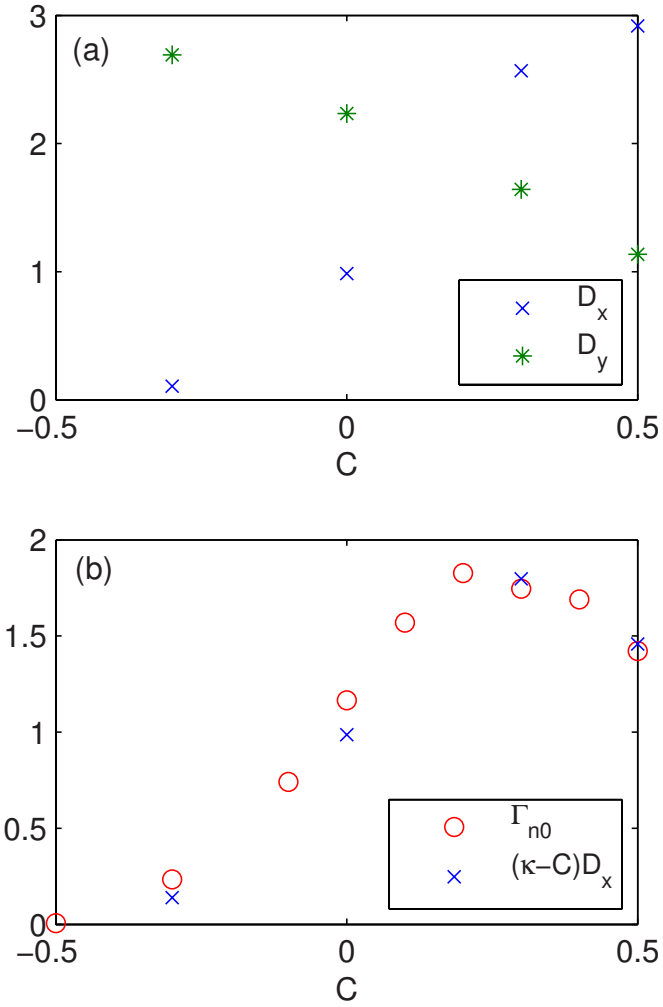

FIG. 7. (Color online) (a) Time independent diffusion coefficients D_x and D_y for different values of C. (b) Average radial density flux Γ_{n0} and $(\kappa-C)D_x$ for different values of C.

that $d\langle x^2\rangle=2D_x dt$, and from Eqs. (7) and (8) and the definition of ζ that $d\langle\zeta^2\rangle=2(\kappa-C)\Gamma_{n0}dt$. Combining these three expressions, we infer

$$\Gamma_{n0}=(\kappa-C)D_x, \tag{25}$$

which is in the form of Fick's law. Since the steady-state value of D_x is found to scale approximately linearly with C, for the values considered in Fig. 7(a) we infer empirically that Eq. (25) is approximately quadratic in C, leading to the maximum in Γ_{n0} seen in Fig. 7(b). In Fig. 7(b) we also plot $(\kappa-C)D_x$ which closely matches Γ_{n0}. Thus we may use Eq. (25) to link the radial diffusive transport of test particles to the underlying turbulence. Since this relation is valid only in the inviscid limit, some departure for larger values of dissipation (D,μ) is expected. We have verified this with our code and, for the case of $C=0$, we obtain results similar to those presented in Ref. 22. For $C=\pm 0.3$ the agreement is similar or better for same range of examined dissipation coefficients. Interestingly, the expression includes the factor $\kappa-C$, which we have shown in Sec. II is related to poloidal flow velocity. Thus the radial diffusion of test particles D_x is linked to the radial turbulent flux Γ_{n0} and poloidal flow. The

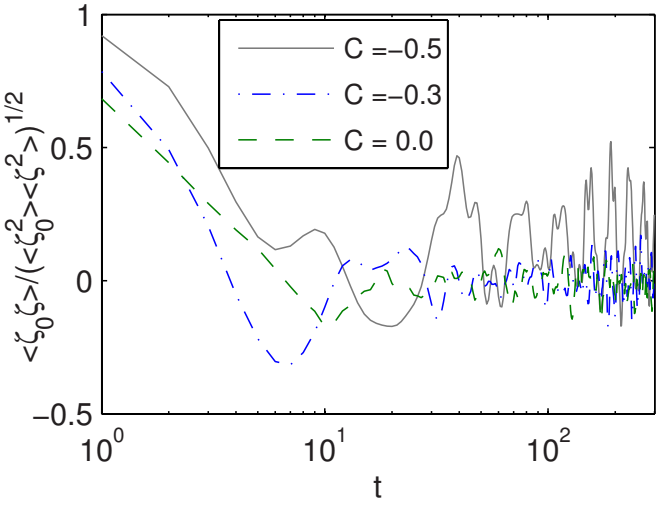

FIG. 8. (Color online) Normalized correlation between fluid potential vorticity ζ_0 at $t=0$ and fluid potential vorticity ζ at time t for different values of C.

effect of a homogeneous poloidal flow on test particle transport was discussed in Ref. 35.

If correlations between ζ and its initial value ζ_0 do not vanish, it follows that $d\langle\zeta^2\rangle$ and hence the diffusion coefficient can be functions of time, leading to nondiffusive transport. In Fig. 8 we show how the normalized correlation $\langle\zeta_0\zeta\rangle/\sqrt{\langle\zeta_0^2\rangle\langle\zeta^2\rangle}$ evolves with time in the saturated turbulent state for $C=[-0.5,-0.3,0]$. In all cases, there is an initial phase where correlations decay, corresponding to the initial ballistic phase of the test particle transport. After this phase, for the $C=-0.3$ and $C=0$ cases, the correlation fluctuates around zero and the test particle transport is diffusive. For the $C=-0.5$ case, however, correlations persist for long times and the test particle transport is nondiffusive.

VI. SUMMARY

We have studied an extended form of the HW model that includes the effects of a magnetic field inhomogeneity in the radial direction $B(x)$. With the parameter controlling the background density gradient set to $\kappa=1$ throughout, we have established that the parameter C, controlling the radial gradient of the magnetic field $B(x)$, alters the properties of the turbulence and the dispersion of test particles. The change in turbulent transport is clearly seen in the distribution of turbulent $E\times B$ density flux $P(\Gamma_n)$. The skewness of the PDF increases with C, with the distribution for $C=-0.3$ being nearly symmetric. Since density n and potential ϕ fluctuations are close to Gaussian, this increase in skewness can be attributed to the increase in phase shifts between n and ϕ, reflecting the transition from drift wave turbulence to drift-interchange-type turbulence. The increase in the skewness also implies an increase in the correlation between fluctuations in density and radial velocity. We have quantified this correlation by examining the dynamics of a single nonlinear monopole structure. The results show that for positive values of C the signs of density and radial velocity fluctuations are the same, increasing the skewness of turbulent flux.

Measurements of diffusion coefficients show that the rate of radial transport of test particles increases and the rate of poloidal transport decreases monotonically with C. For large negative values of C, correlations in the flow persist for long times and the radial transport becomes subdiffusive while the poloidal transport becomes superdiffusive. The rate of radial diffusive test particle transport and the average $E\times B$ density flux can be linked by a simple expression in the form of Fick's law.

ACKNOWLEDGMENTS

This work was supported in part by the UK Engineering and Physical Sciences Research Council and by Euratom. J.M.D. acknowledges the support from an EPSRC CASE studentship in association with UKAEA. The content of the publication is the sole responsibility of the authors and it does not necessarily represent the views of the Commission of the European Union or their services.

[1] G. Y. Antar, G. Counsell, Y. Yu, B. LaBombard, and P. Devynck, Phys. Plasmas **10**, 419 (2003).
[2] B. Ph. van Milligen, R. Sanchez, B. A. Carreras, V. E. Lynch, B. LaBombard, M. A. Pedrosa, C. Hidalgo, B. Goncalves, R. Balbin, and W7-AS Team, Phys. Plasmas **12**, 052507 (2005).
[3] J. P. Graves, J. Horacek, R. A. Pitts, and K. I. Hopcraft, Plasma Phys. Controlled Fusion **47**, L1 (2005).
[4] C. Hidalgo, B. Ph. van Milligen, and M. A. Pedrosa, C. R. Phys. **7**, 679 (2006).
[5] R. O. Dendy and S. C. Chapman, Plasma Phys. Controlled Fusion **48**, B313 (2006).
[6] J. M. Dewhurst, B. Hnat, N. Ohno, R. O. Dendy, S. Masuzaki, T. Morisaki, and A. Komori, Plasma Phys. Controlled Fusion **50**, 095013 (2008).
[7] B. Hnat, B. D. Dudson, R. O. Dendy, G. F. Counsell, A. Kirk, and MAST Team, Nucl. Fusion **48**, 085009 (2008).
[8] W. Horton, Rev. Mod. Phys. **71**, 735 (1999).
[9] A. Hasegawa and M. Wakatani, Phys. Rev. Lett. **50**, 682 (1983).
[10] L. Chen, M. S. Chance, and C. Z. Cheng, Nucl. Fusion **20**, 901 (1980).
[11] H. Sugama, M. Wakatani, and A. Hasegawa, Phys. Fluids **31**, 1601 (1988).
[12] B. D. Scott, New J. Phys. **7**, 92 (2005).
[13] M. Vergote, M. Van Schoor, Y. Xu, S. Jachmich, and R. Weynants, Plasma Phys. Controlled Fusion **48**, S75 (2006).
[14] A. Hasegawa and K. Mima, Phys. Fluids **21**, 87 (1978).
[15] G. Manfredi and R. O. Dendy, Phys. Rev. Lett. **76**, 4360 (1996).
[16] G. Manfredi and R. O. Dendy, Phys. Plasmas **4**, 628 (1997).
[17] S. V. Annibaldi, G. Manfredi, R. O. Dendy, and L. O'C. Drury, Plasma Phys. Controlled Fusion **42**, L13 (2000).
[18] S. V. Annibaldi, G. Manfredi, and R. O. Dendy, Phys. Plasmas **9**, 791 (2002).
[19] K. Gustafson, D. del-Castillo-Negrete, and W. Dorland, Phys. Plasmas **15**, 102309 (2008).
[20] T. S. Pedersen, P. K. Michelsen, and J. Juul Rasmussen, Phys. Plasmas **3**, 2939 (1996).
[21] V. Naulin, A. H. Nielsen, and J. Juul Rasmussen, Phys. Plasmas **6**, 4575 (1999).
[22] R. Basu, T. Jessen, V. Naulin, and J. Juul Rasmussen, Phys. Plasmas **10**, 2696 (2003).
[23] R. Basu, V. Naulin, and J. Juul Rasmussen, Commun. Nonlinear Sci. Numer. Simul. **8**, 477 (2003).
[24] S. Futatani, S. Benkadda, Y. Nakamura, and K. Kondo, Phys. Plasmas **15**, 072506 (2008).
[25] V. Naulin, J. Juul Rasmussen, C. Angioni, C. Giroud, M. Valisa, M. E. Puiatti, and L. Carraro, AIP Conf. Proc. **1013**, 191 (2008).
[26] V. Naulin, O. E. Garcia, M. Priego, and J. Juul Rasmussen, Phys. Scr., T **T122**, 129 (2006).

[27]C. Angioni and A. G. Peeters, Phys. Plasmas **15**, 052307 (2008).
[28]G. E. Karniadakis, M. Israeli, and S. O. Orzag, J. Comput. Phys. **97**, 414 (1991).
[29]A. Arakawa, J. Comput. Phys. **1**, 119 (1966).
[30]V. Naulin, Phys. Plasmas **10**, 4016 (2003).
[31]V. Naulin and A. Nielsen, SIAM J. Sci. Comput. (USA) **25**, 104 (2003).
[32]B. D. Scott, AIP Conf. Proc. **1013**, 316 (2008).
[33]B. A. Carreras, C. Hidalgo, E. Sanchez, M. A. Pedrosa, R. Balbin, I. Garcia-Cortes, B. Ph. van Milligen, D. E. Newman, and V. E. Lynch, Phys. Plasmas **3**, 2664 (1996).
[34]V. Naulin, New J. Phys. **4**, 28 (2002).
[35]T. Hauff and F. Jenko, Phys. Plasmas **14**, 092301 (2007).